Sakarya University Journal of Science 25(5), 1197-1209, 2021

Self-tuning fuzzy logic control of quarter car and bridge interaction model

Mustafa EROĞLU*[1], Mehmet Akif KOÇ[2], Recep KOZAN[1], İsmail ESEN[3]

Abstract

In this study, active suspension control of the interaction between the bridge can be modeled according to the Euler-Bernoulli beam theory, and the quarter car model with three degrees of freedom is studied. The active suspension system consists of a spring, damper, and linear actuator. The active suspension control is designed using classical PID and self-tuning fuzzy PID (STFPID) to reduce the vehicle body's disruptive effects. To determine the performance of the designed controllers, two different road profiles with the bridge oscillations caused by the bridge flexibility were considered as the disruptive effect of the vehicle. When the simulation results were examined in terms of passenger seat displacement and acceleration, the proposed STFPID method significantly increased road holding and ride comfort.

Keywords: Active vibration control, Quarter car model, Fuzzy logic, PID

1. INTRODUCTION

Suspension systems in vehicles are positioned between the wheels and the vehicle body. The suspension system generally consists of spring, damping, and their connections. The primary purpose of the suspension systems is to absorb the adverse effects that affect the vehicle. In this context, it is studied on the damping of vehicle vibrations in the automotive industry and academic studies. Car models can generally be modeled a quarter, half, and full car models. The suspension system can be divided into three categories: passive, semi-active, and active suspension. In classical passive suspensions, spring and damping coefficients are constant, and they are successful to a limited extent. Therefore, an active suspension system is preferred for efficient damping in different conditions. Vehicle vibrations adversely affect passenger comfort and road holding. In order to improve these negatively affected parameters, active vibration control is performed with linear actuators added to the passive suspensions system. In the active vibration control, the system's acting force is determined and applied by the controller at the desired performance.

There are several approaches to increase the performance of the active controller. Many researchers have preferred PID control in the last

* Corresponding author: mustafaeroglu@sakarya.edu.tr
[1] Sakarya University, Mechanical Engineering.
E-Mail: kazan@sakarya.edu.tr
ORCID: https://orcid.org/0000-0002-1429-7656, https://orcid.org/0000-0001-8544-883X
[2] Sakarya University of Applied Sciences, Faculty of Technology, Department of Mechatronics Engineering.
E-Mail: makoc@subu.edu.tr
ORCID: https://orcid.org/0000-0001-7461-9795
[3] Karabuk University, Faculty of Engineering, Mechanical Engineering.
E-Mail: iesen@karabuk.edu.tr
ORCID: https://0000-0002-7853-1464

decades, which ease to design and has good performance. Güçlü has used a PID controller to increase driving comfort in full car models that he modeled as linear and nonlinear [1]. In Koç's study, an active suspension system with fuzzy logic controller has been modeled to reduce excessive vibrations in the train component[2]. The PID controller can be used alone or together with other controllers to improve its performance. The most preferred of these is the Fuzzy PID controller, where the PID coefficients are determined by fuzzy logic. Khodadadi and Ghadiri used fuzzy logic self-tuning PID as active controllers in the active suspension half-car model and compared it with PID, fuzzy logic, and H∞ controllers [3]. Swethamarai and Lakshmi are designed and compared to show the effect on vibration control, thereby increase ride quality for a 3 degree of freedom quarter car model[4]. Min et al. have performed the fuzzy adaptive output feedback control problem for the quarter-vehicle active suspension systems with electromagnetic actuator[5].

In one of their two different studies, Metin and Güçlü improved the passenger and driving comfort of 11 degrees of freedom rail car models with PID and fuzzy logic control separately[6], while in other studies, they compared PID and PID type fuzzy control in 6 degrees of freedom light rail transportation vehicles[7]. In many studies, PID and Fuzzy logic were used together or as separate controllers. In some studies, a hybrid controller that combines PID and fuzzy logic controllers have been used. Demir et al. ensured the ride comfort of the passenger in the half-car model by using a hybrid control approach[8]. Again using a hybrid control approach, Singh and Aggarwal have performed semi-active vibration control of passenger seat vibrations in the quarter car model[9]. Paksoy et al., using full car model with MR damper, performed semi-active control of vehicle vibrations with PID, fuzzy logic, and Self Tuning Fuzzy Logic controller (STFLC), which is a combination of both controllers, and the STFLC has given better results in vibration reduction performance compared to the other two controllers[10].

Another controller that draws attention in active vibration control studies is sliding mode control (SMC), which provides robustness against external and uncertain parameters. Zhang et al. and Bai and Guo showed that the SMC method proposed using a quarter car model achieved a good control performance for the active suspension system[11,12]. Du et al. proposed a terminal SMC approach to deal with the control issue for uncertain, full car active suspension systems [13]. Singh presented the effectiveness of a novel adaptive neuro-fuzzy inference system (ANFIS) based super twisting SMC in vibration suppression in an active quarter car model's suspension system[14].

Another control method is the Linear Quadratic Regulator (LQR). The LQR control theory, which is the optimal control theory, provides a dynamic system's best performance at minimum cost. In this regard, Ben et al. compared passive, semi-active, and active suspension systems in terms of driving safety and road holding using a half car model[15]. They used LQR in the control of the active suspension system and indicated that the proposed method gives better results against random disturbing road input. Agharkakli et al. applied the LQR control technique to the active suspension system using the quarter car model[16]. There has been an improvement in driving comfort and better handling, thanks to active vibration control against different bump inputs.

In addition, static output feedback control [17] and fuzzy logic controller based on particle swarm optimization controllers [18] can be used in the literature to provide vibration control and driving comfort in active suspension systems.

This study's main purpose is to provide active vibration control of the quarter car model with 3 degrees of freedom to increase the ride comfort and road holding by using PID and fuzzy logic. When the literature is examined, in studies conducted to determine vehicle models' dynamic responses, the flexibility of the ground, the vehicle passes through is generally neglected. In this study, the vehicle's passage over a flexible bridge and the disturbance effects on the car from the road while passing are also considered. The

mathematical model of 3 degrees of freedom quarter car model and Euler-Bernoulli bridge beam is obtained. Then, the first two natural frequency and mode shapes of the bridge beam were determined. The critical speeds of the vehicle corresponding to this natural frequency are calculated. The proposed active suspension control effect has been analyzed in detail, disturbing road input and vehicle speed. In this study, with the proposed method, the interaction between the flexible bridge and the car can be analyzed without the need for costly and time-consuming experimental studies.

2. MATHEMATICAL MODELING OF QUARTER CAR AND BRIDGE

In this study, the dynamic interaction between the quarter car model with 3 degrees of freedom and the bridge beam will be examined. Since the car's pitch motion and roll motion are not considered in this model, the quarter model is used, and only the vertical displacements are examined. The quarter car model consists of 3 parts: car body, wheel, and passenger seat. The parameters m_p, m_v, and m_w represent passenger seat mass, car body mass, and wheel mass, respectively. The spring coefficient between the passenger seat and the car body is defined as k_p, the damping coefficient is defined as c_p, the spring coefficient between the car body and the wheel is defined as k_v, the damping coefficient is defined as c_v, and the wheel spring coefficient is defined k_w. The vertical displacement of the passenger seat, the vertical displacement of the vehicle body, and the wheel's vertical displacement are represented as r_p r_v r_w, respectively. Here, the road disturbance is shown as r_d. The bridge beam's oscillations are also added together with the road disturbance as an input of the system. The vertical movement of the bridge, $w_{b(x,t)}$, represents the displacement of any x point of the bridge beam at any t time, regarding the point where the vehicle enters the bridge. V represents the speed of the vehicle, moving at a constant speed. In the model, there is an actuator that can apply vertical force between the car body and the wheel to increase passenger comfort and driving safety. The controller determines this actuator force shown as u.

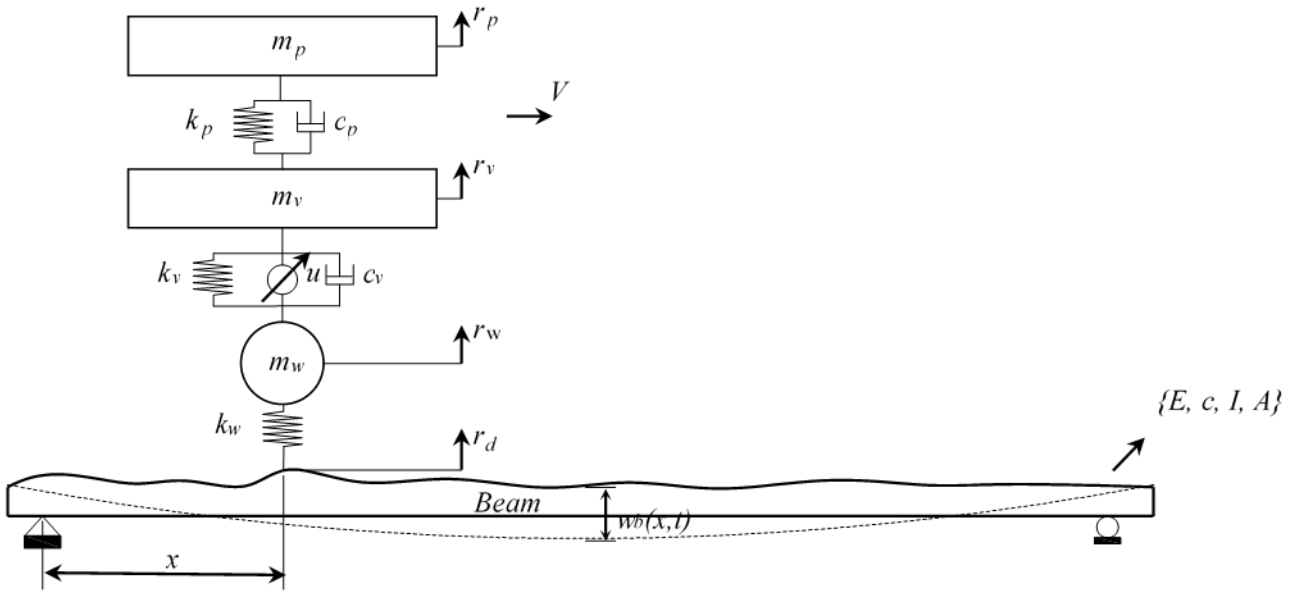

Figure 1 Physical model of the bridge and quarter car model with 3 degrees of freedom.

The natural frequency of vibration modes for the flexible bridge beam shown in Figure 1 is given as in Equation (1) [19].

$$w_j^2 = \frac{j^4 p^4 EI}{mL^4} \ (rad/s) \tag{1}$$

In Equation (1), the parameter ω_j is the circular natural frequency of the bridge beam (rad/s), parameter j represents a number of the mode, the parameter E represents the elastic modulus (N/m^2) of the beam, I represent the moment of inertia (m^4) of the cross-section of the beam. Using Equation (1), the natural frequency of a simply supported beam in Hz is expressed as follows:

$$f_j = \frac{w_j}{2p} = \frac{j^2 p}{2L^2}\left(\frac{EI}{m}\right)^{1/2} \text{ (Hz.)}, \tag{2}$$

The excitation frequency of the vehicle moving on the bridge beam with ω_j natural frequency is expressed as in Equation (3). Using Equation (2), the critical speed of the vehicle is determined as in Equation (4).

$$w = \frac{pv}{L} \tag{3}$$

$$v_{(cr)j} = 2 f_j L = \frac{j^2 p}{L}\left(\frac{EI}{m}\right)^{1/2}, \tag{4}$$

The first two vibration modes of the flexible structure modeled as Euler-Bernoulli beam using the bridge parameters given in Table 1 are f_1=0.1852 Hz, f_2=0.7407 Hz. On the other hand, the vehicle's critical speeds corresponding to these frequencies were determined as V_{cr1}=22.22 m/s, V_{cr2}=88.88 m/s. The following assumptions were accepted in the quarter vehicle and bridge interaction analysis.

- Bridge beam is modeled as a simply-supported beam according to Euler-Bernoulli beam theory.
- Quarter car is modeled with 3 degrees of freedom.
- Only one vehicle passes over the bridge at constant v velocity.
- The car wheel is always in contact with the bridge beam and does not jump.

With these assumptions, the kinetic and potential energies of the quarter car and bridge interaction seen in Figure 1, as well as the damping function, are given in the equations below.

$$E_k = \frac{1}{2}\left[\int_0^L \mu\left[\dot{w}_b^2(x,t)\right]dx + m_p\dot{r}_p^2 + m_v\dot{r}_v^2 + m_w\dot{r}_w^2\right] \tag{5}$$

$$E_p = \frac{1}{2}\left[\int_0^L EI\left[w_b''^2(x,t)\right]dx + k_p(r_p - r_c)^2 + k_v(r_c - r_w)^2 + k_w(r_w - w_b - r_d)^2\right] \tag{6}$$

$$D = \frac{1}{2}\left[\int_0^L c\dot{w}_b^2(x,t)dx + c_p(\dot{r}_p - \dot{r}_c)^2 + c_v(\dot{r}_c - \dot{r}_w)^2\right] \tag{7}$$

In the Equations (5-7), μ is the mass of the unit length of the beam, and EI is the flexural rigidity of the beam. The expression Galerkin for $w_{b(x,t)}$, which is the displacement of any x point on the beam at time t, is given below.

Here q_i represents the generalized coordinate representing the beam element's displacement, φ_i represents the oscillation form obtained with boundary conditions of the bridge beam, and φ_{ij} represents Kronecker delta. The conditions of orthogonality between these oscillation patterns are given in Equation (9). Rayleigh dissipation function for the combined car bridge system is presented in Equation (7). Here c is the equivalent viscous damping coefficient of the bridge beam.

$$\begin{aligned}
&\omega_b(x,t) = \sum_{i=1}^{n}\varphi_i(x)q_i,\\
&\dot{\omega}_b(x,t) = \sum_{i=1}^{n}\varphi_i(x)\dot{q}_i,\\
&\omega_b''(x,t) = \sum_{i=1}^{n}\varphi_i''(x)q_i,\\
&\varphi_i(x) = \sqrt{\frac{2}{L}}\sin\left(\frac{i\pi x}{L}\right), \quad i = 1,2,...,n.
\end{aligned} \tag{8}$$

$$\int_0^L \mu\varphi_i(x)\varphi_j(x)dx = N_i\delta_{ij}, \int_0^L EI\varphi_i''(x)\varphi_j''(x)dx = \Pi_i\delta_{ij} \tag{9}$$

Lagrange expression is the distinction between kinetic energy and potential energies obtained in Equations (5-6). Lagrange expression can be defined as (L=E_k-E_p).

$$\frac{\mathrm{d}}{\mathrm{d}t}\left(\frac{\partial L}{\partial \dot{\eta}_k(t)}\right)-\frac{\partial L}{\partial \eta_k(t)}+\frac{\partial D}{\partial \dot{\eta}_k(t)}=0,\ k=1,2,3 \quad (10)$$

$$\frac{\mathrm{d}}{\mathrm{d}t}\left(\frac{\partial L}{\partial \dot{q}_i(t)}\right)-\frac{\partial L}{\partial q_i(t)}+\frac{\partial D}{\partial \dot{q}_i(t)}=Q_i,\ \mathrm{i}=1,2,3,4 \quad (11)$$

Generalized coordinates are given as in Equations (12-13).

$$\eta(t)=\left\{r_p\ r_v\ r_w\ \right\}^T, \quad (12)$$

$$q(\mathrm{t})=\left\{q_1(\mathrm{t})\ \mathrm{q}_2(\mathrm{t})\ \mathrm{q}_3(\mathrm{t})\ \mathrm{q}_4(\mathrm{t})\ \right\}^T, \quad (13)$$

$$Q_i=\int_0^L \varphi_i(x)\,f_{ci}(x,t)dx,\quad \mathrm{i}=1,..,4 \quad (14)$$

The motion equation of the 3 degrees of freedom quarter car model seen in Figure 1 was obtained using the orthogonality conditions given in Equation (9) and the Galerkin's approach of the beam displacement expressed in Equation (8). Equations of motion for the passenger seat, wheel, and bridge are given below.

$$m_p\ddot{r}_p+c_p(\dot{r}_p-\dot{r}_v)+k_p(r_p-r_v)=0 \quad (15)$$

$$\begin{aligned}&m_v\ddot{r}_v+c_v(\dot{r}_v-\dot{r}_w)-c_p(\dot{r}_p-\dot{r}_v)\\&+k_v(r_v-r_w)-k_p(r_p-r_v)+u=0\end{aligned} \quad (16)$$

$$\begin{aligned}&m_w\ddot{r}_w-c_v(\dot{r}_v-\dot{r}_w)-k_v(r_v-r_w)\\&-k_w(r_w-\varphi_i(x,t)q_i-r_d)-u=0\end{aligned} \quad (17)$$

$$\begin{aligned}&N\ddot{q}_{i(t)}+c\dot{q}_{i(t)}+Sq_{i(t)}\\&-k_w\varphi_i(x,t)(r_w-\sum_{i=1}^{n}\varphi_i(x,t)q_i-r_d)=fg\varphi_i(x,t)\end{aligned} \quad (18)$$

In Equation (18), the second-order equation of the bridge beam is given. Here, f_g value shows the static forces applied to the bridge beam by the car and is calculated as in Equation (19).

$$f_g=(m_p+m_v+m_w)g \quad (19)$$

Table 1 Quarter car and bridge parameters

Parameters of car	
Passenger seat mass (m_p)	80 kg
Car body mass (m_v)	350 kg
Wheel mass(m_w)	40 kg
Stiffness coefficient of primary suspension (k_p)	8000 N/m
Stiffness coefficient of secondary suspension (k_v)	20000 N/m
Tire stiffness (k_w)	180000 N/m
Damping coefficient of primary suspension (c_p)	800 Ns/m
Damping coefficient of secondary suspension (c_v)	1550 Ns/m
Parameters of bridge	
Elasticity module (E)	2.07 GPa
Bridge length (L)	60 m
Cross-section inertia moment (I)	0.17 m^4
Mass of unit length (μ)	2000 kg/m
Equivalent damping coefficient (c)	1750 Ns/m

The quarter car and bridge model's motion equations examined in this study are obtained by the Lagrange method given in Equations (10-11). A total of 7 second-order differential equations, 3 belonging to the car and 4 equations belonging to the bridge, are created. These equations are reduced to 14 first-order differential equations with the help of state-space forms. Then, to solve these equations, the fourth-order Runge Kutta method is used. The dynamic responses that occurred during the car's passage over the bridge, which can be modeled as the Euler-Bernoulli beam, are analyzed with the commercial analysis program MATLAB. The parameters of the car and bridge beam for analysis are given in Table 1.

In this study, an active suspension system is used to increase passenger comfort, which is adversely affected by road irregularity. Road disturbances that adversely affect the vehicle can be in different geometric shapes. In this study, two different road disturbances are added to the system as an input. These are in the form of hump and sinus.

3. DESIGN OF CONTROLLER

Control algorithms designed for active and semi-active suspension systems have been used

extensively in recent years. Active suspension systems are created by adding an actuator to passive suspension systems. The actuator represented by u in Figure 1 provides the necessary vertical force to the system. The controller force is given in Equations (16-17). In this study, car body displacement is used in system feedback to provide the desired performance. Here, car body displacement is expected to be zero displacements.

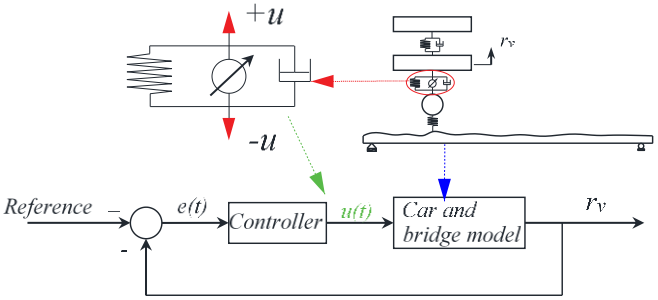

Figure 2 A simple controller design.

In this study, two different controller designs have been made and compared to reduce passenger seat vibrations and displacement in the quarter car model. The first of these is the classic PID controller, which is extensively used in the industry and provides easiness of design. In the classical PID controller, k_p, k_i, and k_d gain parameter values are constant and does not change. The other controller is the Self-tuning Fuzzy PID (STFPID) controller, which allows the classical PID parameters to be adjusted according to stabilization.

3.1. PID Controller

The type of controller with the broadest usage area in the literature is the (Proportional-Integral-Derivative) PID type controller. The PID controller generates a control signal using the error signal of the system. The PID controller is expressed by the equation given in (20).

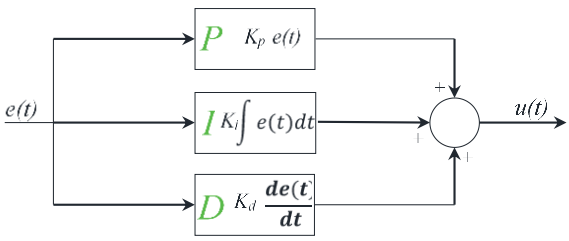

Figure 3 A simple controller design.

$$u = k_p e(t) + k_i \int_0^t e(t)dt + k_d \frac{de(t)}{dt} \qquad (20)$$
$$e(t) = r_r(t) - r_v(t)$$

In the above equation, u, e, r_r, and r_v represent the control force, error signal, a reference displacement value, and actual car body displacement. The coefficients k_p, k_i, and k_d represent the proportional gain, integral gain, and derivative gain of the PID controller.

There are several methods for determining PID controller coefficients. The well-known of these methods is the Ziegler-Nichols method. In this study, the parameters k_p=5*10^4, k_i=1*10^4, k_d=0.5*10^4 are chosen to provide the desired settling time and short rising time.

The proportional gain in the PID control system decreases the rise time of the system, but it may create steady-state error. Integral control negatively affects the transient response while eliminating the steady-state error. Derivative control can predict the future state of the system and correct the transient response. While these controllers can be used alone, they are often used together to increase system stability.

3.2. Self-tuning Fuzzy PID controller

In this section, the self-tuning fuzzy PID (STFPID) controller, which allows the PID gains that determine the controller force to be updated within the system requirements' scope, will be examined. The control gains determined in classical PID control sometimes cannot provide the desired performance while controlling the system. Therefore, fuzzy logic is used to provide the appropriate gains while maintaining the system. In this study, the STFPID controller designed to control the vibration caused by the interaction between the quarter vehicle model and the bridge is shown in Figure 4.

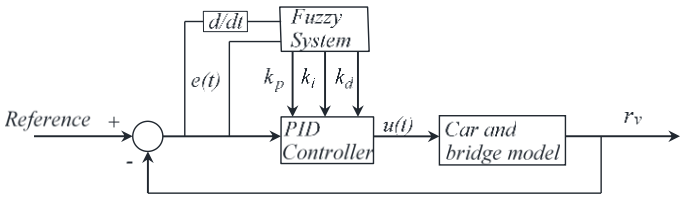

Figure 4 Structure of STFPID control.

The concept of fuzzy logic, which determines how to control a system with the intuitive knowledge of people, was first introduced by Lotfi Zadeh in 1965 [20]. Fuzzy logic consists of 3 different design stages: fuzzification, rule base, and defuzzification. In the fuzzification interface, appropriate linguistic variables are defined for the system inputs examined. The rule base is created by making use of expert experience. In the defuzzification interface, a precise control signal is provided to the active controller using the first two interfaces.

While the fuzzy logic shown in Figure 4 uses the vertical displacement of the vehicle body ($e = r_r - r_v$) and its derivative ($\dot{e} = \dot{r}_r - \dot{r}_v$) as input, it gives the PID parameters as output. Here, reference values ($r_r, \dot{r}_r$) are desired to be zero.

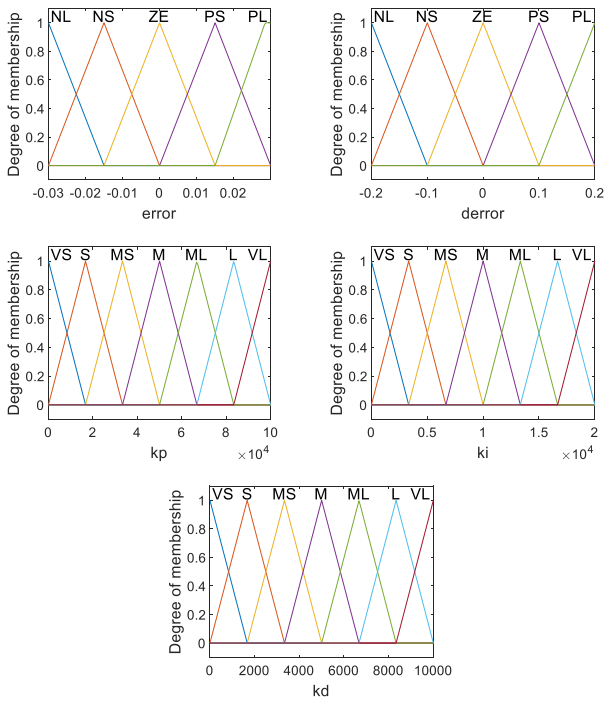

Figure 5 The membership functions of input and output parameters.

The membership functions created for the (STFPID) controller used in this study are shown in Figure 5. As seen in the figure, input values have been represented by five membership functions, namely NL (Negative Large), NS (Negative Small), ZE (Zero), PS (Positive Small), and PL (Positive Large). In comparison, output values have been represented by seven membership functions, namely VS (Very Small), S (Small), MS (Middle Small), M (Medium), ML (Medium Large), L (Large), and VL (Very Large). All membership functions are selected in triangular geometry.

In the input variables given in Figure 5, the membership function of the error is selected in the intervals [-0.03, 0.03], while the change of the error was selected in the intervals of [-0.2, 0.2]. On the other hand, output variables k_p, k_i, and k_d are determined in the ranges [0, 10^5], [0, 2 * 10^4], and [0, 10^4], respectively. The rule base defining the relationship between input and output of these membership functions is given in Table (2-4).

Table 2 Rule base for the k_p

k_p		$\frac{de(t)}{dt}$				
		NL	NS	ZE	PS	PL
$e(t)$	NL	VL	VL	VL	VL	VL
	NS	VL	VL	M	VS	VS
	ZE	VL	ML	M	ML	VL
	PS	MS	M	VL	VL	VL
	PL	ML	L	VL	VL	VL

Table 3 Rule base for the k_i

k_i		$\frac{de(t)}{dt}$				
		NL	NS	ZE	PS	PL
$e(t)$	NL	VL	VL	VL	VL	VL
	NS	VL	VL	ML	VS	VS
	ZE	VL	ML	M	ML	VL
	PS	MS	M	VL	VL	VL
	PL	ML	L	VL	VL	VL

Table 4 Rule base for the k_d

k_d		$\frac{de(t)}{dt}$				
		NL	NS	ZE	PS	PL
$e(t)$	NL	VL	VL	VL	VL	VL
	NS	VL	VL	ML	S	VS
	ZE	VL	L	L	L	VL
	PS	S	M	VL	VL	VL
	PL	VL	VL	VL	VL	VL

4. SIMULATION RESULTS AND DISCUSSION

In this section, the interaction between the quarter car model with 3 degrees of freedom and the bridge that can be modeled according to the simple supported Euler-Bernoulli beam theorem

is examined. For the simulation model, the differential equations given in Equations (15-18) Moreover, the parameters given in Table 1 are taken into account. In the quarter car model, the bridge beam's oscillation is added with two different road inputs as input for the system.

4.1. Bridge displacement input

The bridge is forced to vibrate by the vehicle passing over it at a certain speed. Bridge vibrations also affect the dynamic behavior of the vehicle. In this section, only the bridge beam's oscillations were added to the quarter car as input, and active suspension control was not applied. The parameters of the bridge examined in the simulation are given in Table 1. The modes of the bridge beam, resonance frequencies, and critical speeds of the vehicle are provided in section 1.

In Figure 6, four different velocities, V=54, V=108, V=162, V=216 km/h, are examined. In Figure 6a, when the displacement of the bridge beam midpoint is reviewed, it is seen that the midpoint of the bridge beam makes more displacement at lower speeds of the vehicle. However, as vehicle speed increases, it takes more time for bridge oscillations to damping. In Figures 6b-c, the passenger seat displacement and acceleration values are given, respectively. While the passenger seat displacement values are similar to the bridge midpoint's displacement, the acceleration values and oscillations increase as the speed increases. It is seen that the maximum displacement time of the bridge and the passenger seat rises as the vehicle's speed increases. It is also observed that passenger vertical acceleration values due to bridge flexibility exceed the accepted comfort standards with the increase of vehicle speed. According to the ISO 2631 standard, the low comfort acceleration value that affects the human being is 0.49 m/s^2, and the medium comfortable acceleration value is 0.37 m/s^2 [21].

Figure 7a shows the displacement of the midpoint of the bridge beam, the vertical displacement of the passenger seat, and the passenger seat's vertical acceleration when the vehicle speed changes from 1 m/s to 100 m/s in 1 m/s interval.

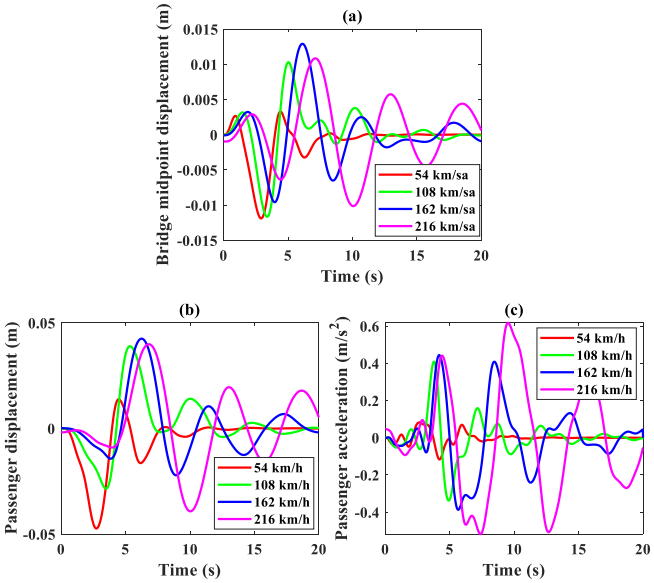

Figure 6 Dynamic responses of quarter car for bridge oscillation (a) Bridge midpoint displacement (b) Passenger displacement (c) Passenger acceleration.

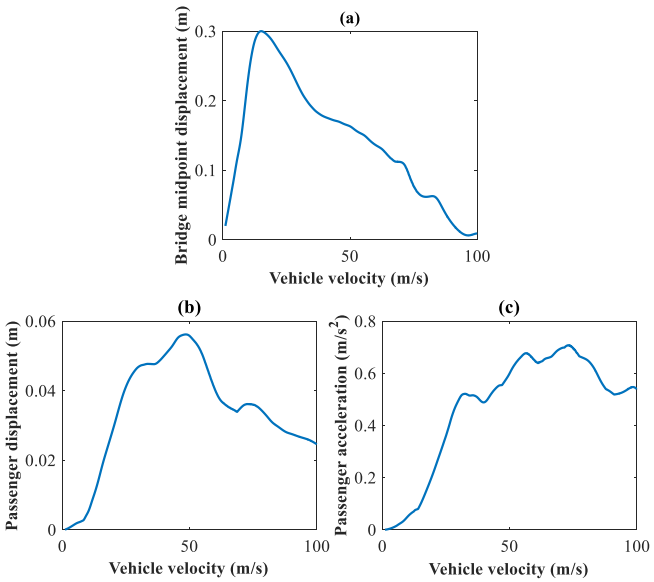

Figure 7 The effect of car velocity upon dynamic response (a) Bridge midpoint displacement (b) Passenger displacement (c) Passenger acceleration.

In Figure 7a, the maximum displacement of the bridge midpoint is determined as 0.3 m when the vehicle speed is 15 m/s. In Figure 7b, if the vehicle speed is approximately 50 m/s, the passenger seat displacement takes its maximum value. At more or less than this speed, the maximum displacement values decrease. In Figure 7c, as the vehicle speed increases, the passenger seat's acceleration values increase, and the acceleration values occurring at speeds above

40 m/s exceed the vibration values affecting humans according to ISO 2631 standard.

4.2. Sinusoidal input

As seen in Figure 8, a sinusoidal input with an amplitude of 0.02 m and a frequency of 3.14 rad/s is applied to the quarter car model for the vehicle's passage across the bridge of 60 m length. Sinusoidal input and bridge displacement input is given as disturbing input to the quarter car. The active controller's performance has been investigated using PID and STFPID controllers for passenger seat displacement and acceleration against disturbance input.

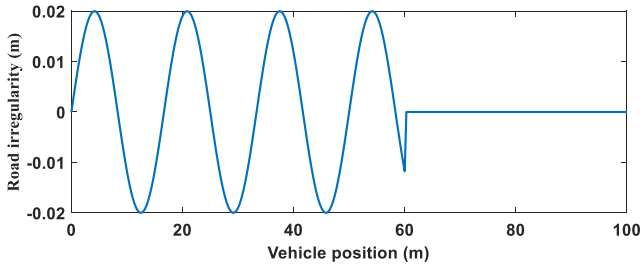

Figure 8. Sinusoidal input.

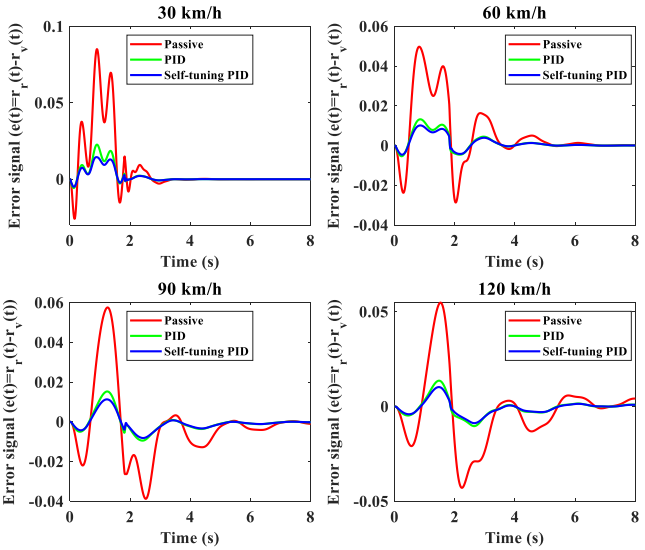

Figure 9 Error signal of car body for a sinusoidal input.

In order to increase passenger comfort in the 3 degree of freedom vehicle model, the vertical displacements of the vehicle body are aimed to be zero. Therefore, the control signal is generated by using the vertical displacements of the vehicle body. In Figure 9, the error signal graph obtained at different vehicle speeds for the sinusoidal input is given. According to the graph, when PID and STFPID controllers are used, it is seen that the error signal value of the vehicle body is considerably reduced compared to the passive control.

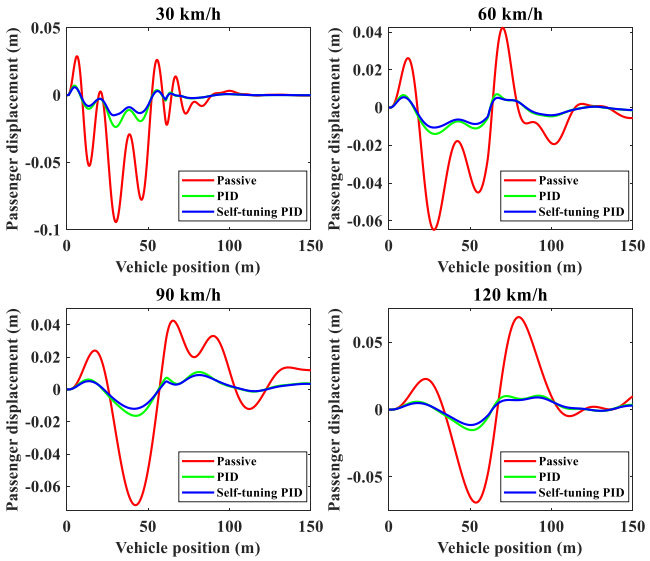

Figure 10 The response of passenger seat displacement for a sinusoidal input.

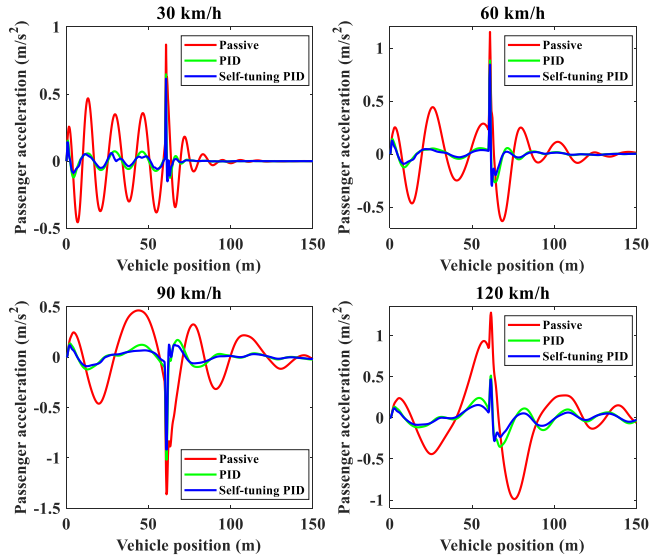

Figure 11 Response of passenger seat acceleration for sinusoidal input.

Figures 10-11 shows the effect of four different vehicle speeds, 30, 60, 90, and 120 km/h, on passenger seat displacement and acceleration. According to the graphics, it is seen that the STFPID controller gives better results than both the PID controller and the uncontrolled system. While the displacement values were relatively high in the simulation studies without a controller,

they decreased thanks to the PID, especially the STFPID controller. Also, in Figure 11, the passenger seat's acceleration values exceed the acceleration values affecting humans according to ISO 2631 standard. Figure 12 shows the control forces generated for STFPID and PID controllers.

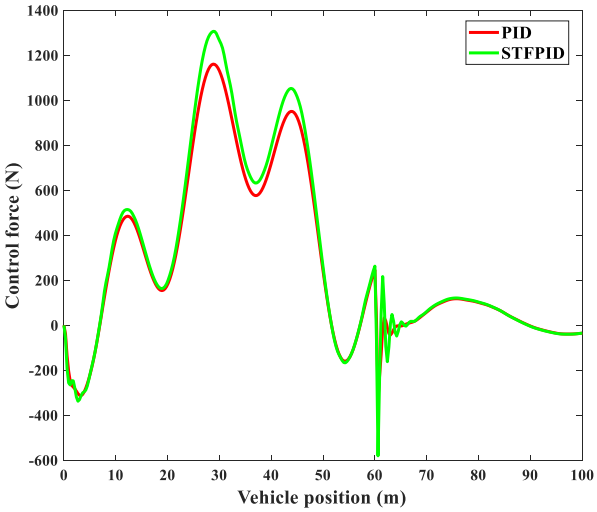

Figure 12 Control force for hump input.

4.3. Hump input

When the quarter car model with 3 degrees of freedom in Figure 1 passes over the bridge, it is exposed to two bumps with a height of 10 cm and a width of 5 m. These hump inputs shown in Figure 13 are located 20 m and 50 m away from the bridge's left reference. The equations of these inputs are determined according to the height and width of the hump and the vehicle's speed and are calculated in Equation (21) Here, the expression Y represents the height of the hump, ω represents the angular frequency, and r_d represents the value of the hump at time t. T time is calculated as the time the vehicle passes the hump.

$$r_d = Y\sin(\omega t), \qquad 0 \le t \le T, \qquad T = \frac{L}{V} \qquad (21)$$

In this case, the frequency of the sine wave given for the hump is as follows.

$$\omega = \frac{\pi V}{L} \qquad (22)$$

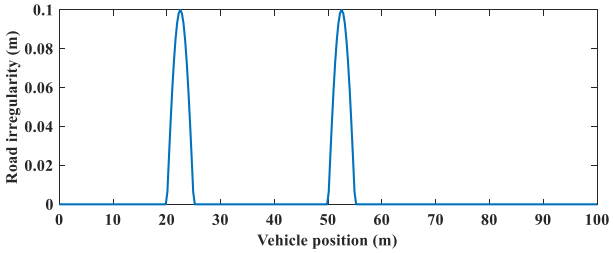

Figure 13 Hump input.

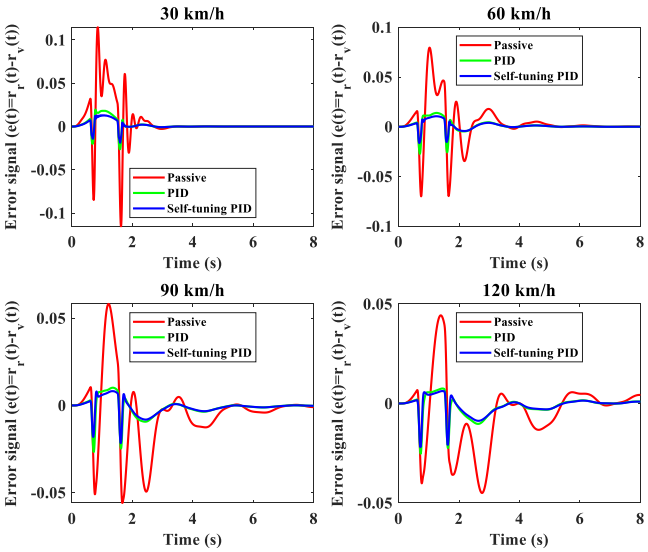

Figure 14 Error signal of car body for hump input.

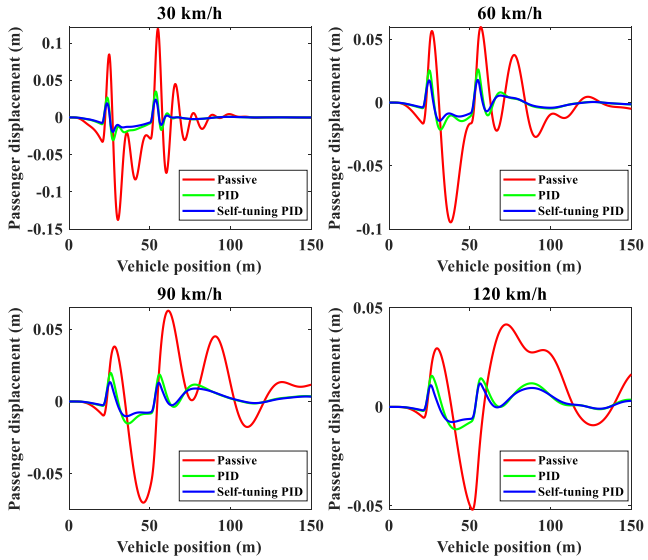

Figure 15 The response of passenger seat displacement for hump input.

In Figure 14, the error signal graph of the vehicle body is given for the hump input. According to the graph, if a controller is used, as in Figure 9, the error signal of the vehicle body is considerably reduced. In Figures 15-16, the controllers' performance proposed in this study for the hump input in passenger seat displacement and

acceleration values is examined. Like the sinusoidal input, four different speeds were evaluated and compared with STFPID and PID controllers. If the vehicle speed is 30 km/h, it is seen that the vertical displacement of the passenger seat is approximately 0.1 m, while it is about 0.05 m at other speeds. Thanks to the active suspension control, these relatively high displacement values have been reduced to very reasonable levels. In the case of increased vehicle speed, the passenger seat's vertical acceleration values also increase considerably. In Figure 17, both controller forces generated corresponding to the input values with hump and bridge displacement are given.

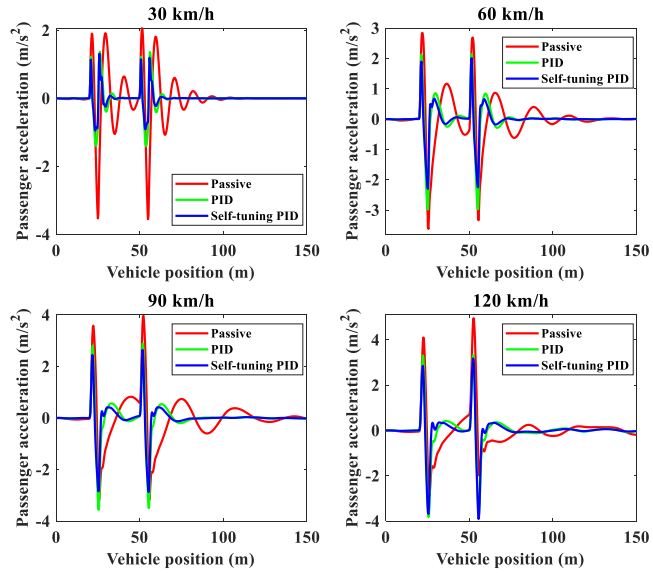

Figure 16 The response of passenger seat acceleration for hump input.

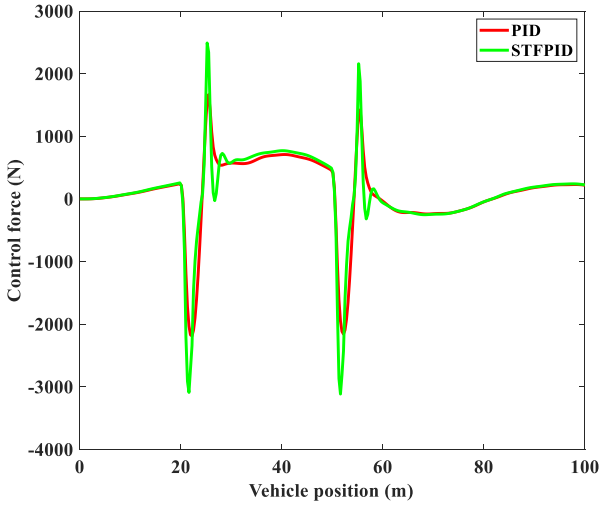

Figure 17 Control force for hump input.

5. CONCLUSION

In this study, it is investigated that disturbing road irregularities, which adversely affect the driving safety and passenger comfort parameters of the quarter car model, will be absorbed by the active suspension system. Modeled 3 degrees of the freedom car model were examined with uncontrolled and STFPID and PID type controllers. Uncontrolled and controlled systems are compared with each other using different system inputs. In the simulation results, it was determined that the STFPID controller performs much better than the others.

Table 5 RMS results for error signal ($e(t)=r_r(t)-r_v(t)$)

	Hump input (m)				Sinusoidal input (m)			
	30 km/h	60 km/h	90 km/h	120 km/h	30 km/h	60 km/h	90 km/h	120 km/h
Passive	0.0227	0.0189	0.0180	0.0163	0.0192	0.0156	0.0176	0.0181
PID	0.0055	0.0050	0.0048	0.0046	0.0052	0.0041	0.0045	0.0044
Self-tuning FPID	0.0039	0.0036	0.0039	0.0040	0.0038	0.0033	0.0036	0.0036
Improvement	27.96%	28.34%	18.72%	12.55%	27.56%	18.77%	18.93%	17.49%

Table 6. RMS results for passenger displacement

	Hump input (m)				Sinusoidal input (m)			
	30 km/h	60 km/h	90 km/h	120 km/h	30 km/h	60 km/h	90 km/h	120 km/h
Passive	0.0256	0.0205	0.0208	0.0167	0.0208	0.0178	0.0207	0.0234
PID	0.0064	0.0056	0.005	0.0047	0.0054	0.0043	0.0049	0.0049
Self-tuning FPID	0.0045	0.0041	0.0038	0.0037	0.0039	0.0035	0.0039	0.004
Improvement	29.3%	27.4%	24.3%	21.7%	28%	19.2%	20%	19.1%

Table 7 RMS results for passenger acceleration

	Hump input (m/s^2)				Sinusoidal input (m/s^2)			
	30 km/h	60 km/h	90 km/h	120 km/h	30 km/h	60 km/h	90 km/h	120 km/h
Passive	0.5161	0.5599	0.6503	0.6322	0.1345	0.1638	0.2071	0.3004
PID	0.2288	0.3865	0.5685	0.5327	0.0357	0.0567	0.0733	0.0872
Self-tuning FPID	0.1667	0.2987	0.3858	0.5021	0.0298	0.0493	0.06	0.0631
Improvement	27.2%	22.7%	17.6%	5.7%	16.3%	13.1%	17.2%	27.6%

This study's primary purpose is to reduce the passenger seat's displacement and acceleration values through controllers. In this context, error signal of car body, the passenger seat displacement, and acceleration values are compared under different speeds and disturbance inputs in Table (5-7). Root mean square (RMS) values of the uncontrolled results with both controllers are given in the table for comparison. After comparing the classical PID controller and the STFPID controller, the simulation results show that the STFPID controller has achieved more than 20% improvement over the classic PID controller.

REFERENCES

[1] R. Güçlü, "Active control of seat vibrations of a vehicle model using various suspension alternatives," Turkish J. Eng. Environ. Sci. 27 (2003) 361–373. https://doi.org/10.3906/sag-1204-7.

[2] M.A. Koç, "Dynamic Response and Fuzzy Control of Half-Car High-Speed Train and Bridge Interaction," Acad. Perspect. Procedia. 3 (2020) 519–529. https://doi.org/10.33793/acperpro.03.01.100.

[3] H. Khodadadi, and H. Ghadiri, "Self-tuning PID controller design using fuzzy logic for half car active suspension system," Int. J. Dyn. Control. 6 (2018) 224–232. https://doi.org/10.1007/s40435-016-0291-5.

[4] P. Swethamarai, and P. Lakshmi, "Design and implementation of fuzzy-PID controller for an active quarter car driver model to minimize driver body acceleration," IEEE Int. Syst. Conf. (2019) 1–6. https://doi.org/10.1109/SYSCON.2019.8836940.

[5] X. Min, Y. Li, and S. Tong, "Adaptive fuzzy output feedback inverse optimal control for vehicle active suspension systems," Neurocomputing. 403 (2020) 257–267. https://doi.org/10.1016/j.neucom.2020.04.096.

[6] M. Metin, and R. Guclu, "Active vibration control with comparative algorithms of half rail vehicle model under various track irregularities," JVC/Journal Vib. Control. 17 (2011) 1525–1539. https://doi.org/10.1177/1077546310381099.

[7] M. Metin, and R. Güçlü, "Vibrations control of light rail transportation vehicle via PID type fuzzy controller using parameters adaptive method," Turkish J. Electr. Eng. Comput. Sci. 19 (2011) 807–816. https://doi.org/10.3906/elk-1001-394.

[8] O. Demir, I. Keskin, and S. Cetin, "Modeling and control of a nonlinear half-vehicle suspension system: A hybrid fuzzy logic approach," Nonlinear Dyn. 67 (2012) 2139–2151. https://doi.org/10.1007/s11071-011-0135-y.

[9] D. Singh, and M.L. Aggarwal, "Passenger seat vibration control of a semi-active quarter car system with hybrid Fuzzy–PID approach", Int. J. Dyn. Control. 5 (2017) 287–296. https://doi.org/10.1007/s40435-015-0175-0.

[10] M. Paksoy, R. Guclu, and S. Cetin, "Semiactive self-tuning fuzzy logic control of full vehicle model with MR damper,"" Adv. Mech. Eng. 2014 (2014). https://doi.org/10.1155/2014/816813.

[11] Y.Q. Zhang, Y.S. Zhao, J. Yang, and L.P. Chen, "A dynamic sliding-mode controller with fuzzy adaptive tuning for an active suspension system," Proc. Inst. Mech. Eng. Part D J. Automob. Eng. 221 (2007) 417–428. https://doi.org/10.1243/09544070JAUTO379.

[12] R. Bai, and D. Guo, "Sliding-mode control of the active suspension system with the dynamics of a hydraulic actuator," Complexity. 2018 (2018). https://doi.org/10.1155/2018/5907208.

[13] M. Du, D. Zhao, B. Yang, and L. Wang, "Terminal sliding mode control for full vehicle active suspension systems," J. Mech. Sci. Technol. 32 (2018) 2851–2866. https://doi.org/10.1007/s12206-018-0541-x.

[14] D. Singh, "Passenger body vibration control in active quarter car model using ANFIS based super twisting sliding mode controller," Simul. Model. Pract. Theory. 89 (2018) 100–118. https://doi.org/10.1016/j.simpat.2018.09.010.

[15] L.Z. Ben, F. Hasbullah, and F.W. Faris, "A comparative ride performance of passive, semi-active and active suspension systems for off-road vehicles using half car model," Int. J. Heavy Veh. Syst. 21 (2014) 26–41. https://doi.org/10.1504/IJHVS.2014.057827.

[16] A. Agharkakli, G.S. Sabet, and A. Barouz, "Simulation and Analysis of Passive and Active Suspension System Using Quarter Car Model for Different Road Profile," Int. J. Eng. Trends Technol. 3 (2012) 636–644.

[17] J. Mrazgua, R. Chaibi, E.H. Tissir, and M. Ouahi, "Static output feedback stabilization of T-S fuzzy active suspension systems," J. Terramechanics. 97 (2021) 19–27. https://doi.org/10.1016/j.jterra.2021.05.001.

[18] G.I.Y. Mustafa, H.P. Wang, and Y. Tian, "Vibration control of an active vehicle suspension systems using optimized model-free fuzzy logic controller based on time delay estimation," Adv. Eng. Softw. 127 (2019) 141–149. https://doi.org/10.1016/j.advengsoft.2018.04.009.

[19] L. Frýba, "Vibration of Solids and Structures under Moving Loads," 3rd ed., Thomas Telford, London, ISBN 0-7277-2741-9, (1999).

[20] L. A. Zadeh, "Fuzzy sets," Information and Control (1965) 338–353. https://www.sciencedirect.com/science/article/pii/S001999586590241X.

[21] C. Mizrak, and I. Esen, "Determining Effects of Wagon Mass and Vehicle Velocity on Vertical Vibrations of a Rail Vehicle Moving with a Constant Acceleration on a Bridge Using Experimental and Numerical Methods," Shock Vib. 2015 (2015). https://doi.org/10.1155/2015/183450.